World Academy of Science, Engineering and Technology
International Journal of Electronics and Communication Engineering
Vol:1, No:6, 2007

Energy-Efficient Sensing Concept for a Micromachined Yaw Rate Sensor

D. Oshinubi, M. Rocznik, and K. Dostert

***Abstract*—**The need for micromechanical inertial sensors is increasing in future electronic stability control (ESC) and other positioning, navigation and guidance systems. Due to the rising density of sensors in automotive and consumer devices the goal is not only to get high performance, robustness and smaller package sizes, but also to optimize the energy management of the overall sensor system. This paper presents an evaluation concept for a surface micromachined yaw rate sensor. Within this evaluation concept an energy-efficient operation of the drive mode of the yaw rate sensor is enabled. The presented system concept can be realized within a power management subsystem.

***Keywords*—**inertial sensors, micromachined gyros, gyro sensing concepts, power management, FPGA

I. Introduction

INERTIAL sensors are used in any application that requires the measurement of rotation, rotation rate or acceleration. Conventional macro-technology gyroscopes like mechanical or optical concepts [1], [2] require a large package, are heavy and very costly. The technology for microelectromechanical systems (MEMS) has the advantage that it allows production in high volumes on silicon wafers with the benefit of small size and low fabrication costs. Micromachined inertial sensors are one of the most important types of silicon-based sensors. The fabrication technologies for MEMS are being intensely developed for the last years and are a focus of research worldwide and further the manufacturing of micromachined yaw rate sensors in a surface micromachining process is well known [3], [4], [5].

The system realization presented in this paper, is based on a capacitive silicon surface micromachined yaw rate sensor [6]. The sensor is targeting systems like electronic stability program (ESP), electronic active steering (EAS), roll over mitigation (ROM), active suspension control (ASC), steer by wire (SbW) and other advanced vehicle stabilizing systems. The focus is on a sensing concept to reduce the power consumption of the whole sensor. The idea is to decrease the current consumption of the analog frontend by reducing the operating time of the analog frontend's components such as capacity to voltage (C/V)-converters, analog digital (A/D)-converters, charge pumps or other controllers which are driven continuously for state of the art sensors.

The presented scheme is able in combination with a capacitive micromechanical yaw rate sensor including a high quality factor of the drive path and an advanced power management subsystem to decrease the average time during which current is consumed by the analog frontend. Thus a power efficient operation can be enabled. The system approach was implemented in a compact field programmable gate array (FPGA) board which contains an analog frontend on the top to preprocess the small capacitance signals of the sensor element and a FPGA on the bottom to evaluate the derived system algorithm in real-time.

D. Oshinubi and M. Rocznik are with Corporate Sector Research and Advance Engineering, Robert Bosch GmbH Gerlingen, Germany
K. Dostert is professor at the Institute of Industrial Information Technology, University of Karlsruhe, Germany

II. Angular Rate Sensor Element

The angular rate sensor MM3 [6] is produced with surface micromachining. The sensor element is shown in Fig. 1.

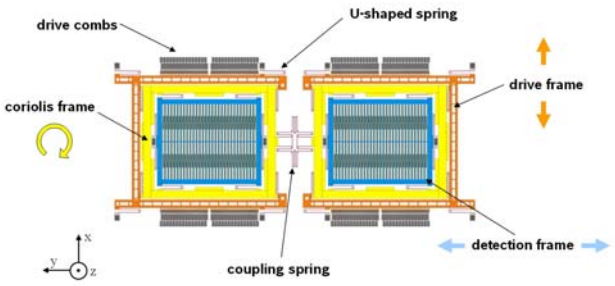

Fig. 1. Schematic view of the micromechanical z-axis sensitive sensor element

The actuation of the drive frame is realized using electrostatic forces and the evaluation of the detection frame is realized via electrostatic finger electrodes.

The sensor element consists of two identical structures which are connected through a coupling spring. This coupling spring and the two identical structures are needed to suppress occurring linear accelerations. Each of these structures contains three frames shown in Fig. 1. The drive frame, the Coriolis frame and the detection frame. Each frame is connected to another via U-shaped springs. To get the sensor into operation mode, the drive frames are excited to a resonant vibration at approximately 15 kHz, by the electrostatic comb drives along the x-axis. The U-shaped springs transfer the drive motion to the Coriolis frame. The U-shaped springs between the Coriolis frame and the detection frame are used to decouple the drive motion from the detection motion of the sensor element. An external angular rate along the z-axis can be measured by translating the occurring Coriolis accelerations, at the Coriolis frame, into a motion along the y-axis of the detection frame.

The resulting Coriolis force is described by

$$\vec{F_c} = 2m\left(\vec{v} \times \vec{\Omega}\right) \tag{1}$$

In (1) $\vec{F_c}$ denotes the resulting Coriolis force, m the mass of the proof mass, $\vec{v}$ the velocity of the proof mass and $\vec{\Omega}$ the present angular rate. The motion of the detection frame leads to a change of the detection capacitances, which are proportional to the present angular rate along the z-axis. A more detailed description can be found in [6], [1].

III. SIGNAL PROCESSING

For further system examination, the drive path of the sensor is considered in more detail. Fig. 2 shows the block diagram of the drive path and how it is realized here. The change of the detection capacity of the drive comb electrodes is converted to a voltage signal via a C/V-converter. Then the voltage signal is digitized through an A/D converter, digitally processed and finally fed back to the sensor drive path.

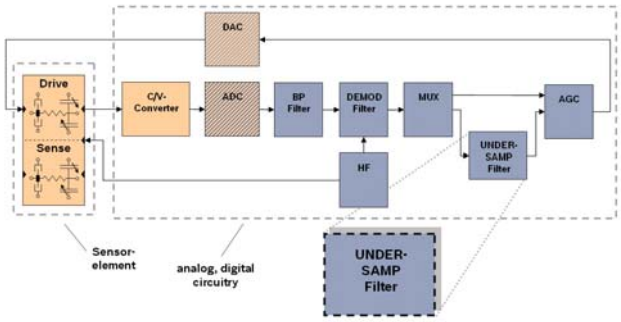

Fig. 2. Block diagram of the sensing concept for the drive path with the under-sampling filter

To evaluate the Coriolis accelerations, a sinusoidal velocity of the drive frame is needed. The present state of the detection frame is measured through the analog frontend which operates with a carrier frequency sensing principle. The actual signal processing such as bandpass filtering, demodulation and automatic gain control (AGC) is done within the digital circuitry of the FPGA. Inside the FPGA the detection signal of the drive frame is bandpass filtered, demodulated and fed back to the comb electrodes of the drive frame. The feedback is done after calculating the actual values to continue the drive frame oscillation with a constant amplitude within the AGC. Fig. 2 shows the possibility to switch between the regular drive mode concept and the under-sampling drive mode concept through a multiplexer. To examine the new system approach a reduction of the sample frequency through down and up sampling within the UNDER-SAMP-filter block is used.

The concept presented in this paper is based on the principle that the excitation of the drive signal is not sampled like usual with a sampling frequency higher than twice the highest signal frequency component to avoid aliasing. Rather, the sampling frequency is intentionally set lower to make use of the appearing alias components. The time domain signals after undersampling are shown in Fig. 3. They are calculated for 3 different values of f_A. The resulting different aliasing signals are interpolated between the discrete samples to show time continuous behavior.

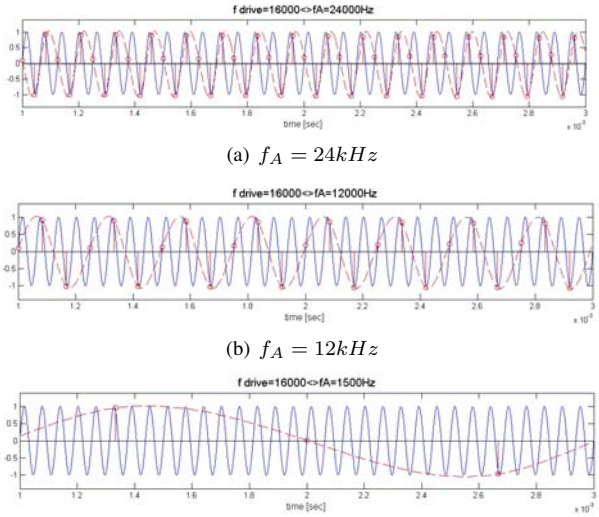

(a) $f_A = 24kHz$

(b) $f_A = 12kHz$

(c) $f_A = 1.5kHz$

Fig. 3. Time domain of the appearing aliasing signals after under-sampling the drive signal with different sampling frequencies

If the drive signal $s_{drive}(t)$ is sampled with the sampling time t_A, we get a sampled sequence according to [8]

$$s_{drive*}(t) = \sum_{n=-\infty}^{n=+\infty} \delta(t - nt_A) \tag{2}$$

When the drive signal $s_{drive*}(t)$ given in equation (2) is Fourier transformed into the frequency domain the following relation results:

$$S_{drive*}(f) = f_A \sum_{k=-\infty}^{k=+\infty} S_{drive}(f - kf_A) \tag{3}$$

For the case treated in this paper, the drive signal $s_{drive}(t)$ is assumed to be a real cosine function. Therefore, the subsequent transform is valid.

$$\cos(2\pi f_0 t) \circ\!\!-\!\!\bullet \frac{1}{2}\left[\delta(f + f_0) + \delta(f - f_0)\right] \tag{4}$$

If equation (4) is used to determine the spectrum described in equation (3) we get the result in equation (5).

$$S_{sub}(f) = f_A \sum_{k=-\infty}^{k=+\infty} \frac{1}{2}\left[\delta(f + f_0 - kf_A) + \delta(f - f_0 - kf_A)\right] \tag{5}$$

Likewise it is possible to realize a rational proportion between f_{sub} and f_{drive}, but we further assume that the resulting frequency component f_{sub} through under-sampling complies with the conditions

$$\begin{aligned} f_{sub} &= 2^{-m} \cdot f_{drive} \\ |f_{sub}| &\leq \frac{f_A}{2} = f_N \end{aligned} \tag{6}$$

After solving the above mentioned equation (5) for f_A we get the following possible sampling frequencies f_{Ai} shown in Fig. 4 and Fig. 5. Fig. 4 shows an interpolated plot of the possible sample frequencies without fulfilling equation (6).

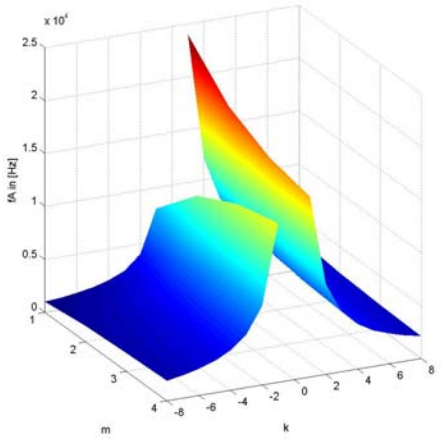

Fig. 4. Calculated sample frequencies for under-sampling without restriction for f_{sub}

In Fig. 5 only those sample frequencies f_{Ai} are depicted which meet equation (6).

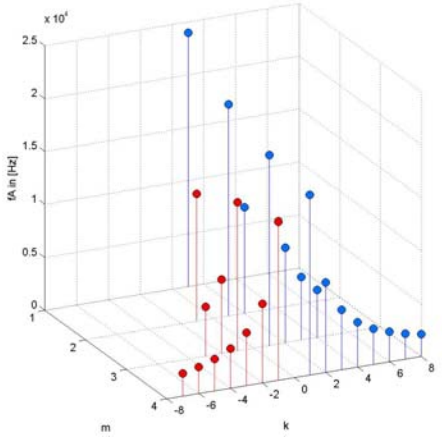

Fig. 5. Valid sample frequencies for under-sampling restricted through equation (6)

Fig. 6 contains schematically the positions of the appearing frequencies in the frequency domain. In the shown case, the signal frequency of the cosine oscillation by the drive frame is chosen to be $f_0 = 16kHz$. The sampling frequency is set to $f_A = 24kHz$. The dashed line at $f = f_N$ marks the Nyquist frequency, which would be given by sampling with the sampling frequency f_A and has the value $f_A/2$. In Fig. 6 (above) the sampling frequency is set to a value higher than f_0 but below $2f_0$ (as it would be required by the Nyquist theorem). It would also be possible to choose a value below f_0 as calculated and shown in Fig. 4 and Fig. 5. The spectrum after sampling around zero frequency is shown in Fig. 6 (below). It can be seen that the frequency components of f_0 after under-sampling are appearing in the low pass region through periodic repetition.

The frequency around the Nyqiust band $f_N = 12kHz$ at $f_{sub1} = 8kHz$ is relevant for further processing.

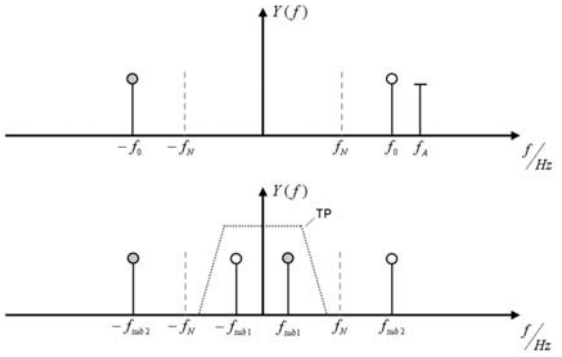

Fig. 6. Appearing frequencies before (above) and after (below) under-sampling

Both frequencies f_{sub1} and f_{sub2} contain information about the drive signal $s_0(t)$. For further steps, the frequency f_{sub1} is filtered out by a digital low pass filter, to extract the designated signal components. The signal $s_{sub1}(n)$ is passed to a digital reconstruction filter, which operates basically with two numerically controlled oscillators (NCO). The schematic overview of the digital reconstruction filter is presented in Fig. 7.

The configuration consists of a phase detector PD, a loop filter SF and the two numerical oscillators NCO1 and NCO2. The phase detector is a phase-frequency detector (PFD) [7] which can determine phase and frequency difference between the two input signals. The PFD has the advantage that its signal output is dependent on the angular frequency if the phase locked loop (PLL) is unlocked and depends on the phase error if the PLL is locked. Compared to other phase detectors, the PFD exhibits the largest hold range. The output of the phase detector is a pulse-width modulated signal. It can operate in three states so that the output values are 0, +1 or -1. To get a valid signal for the NCOs, the output signal of the phase detector needs to be low pass filtered. This task is done by a digital PI-controller.

The two NCOs are set to the center frequencies $f_{NCO1} = f_{sub1} = 8kHz$ and $f_{NCO2} = f_{drive} = 16kHz$ in the given case. NCO1 works together with the phase detector and the loop filter, like a PLL and synchronizes on the under-sampled signal $s_{sub}(n)$ of the drive frame at approximately 8 kHz. If the PLL is synchronized, the signal $s_{sub}(n)$ generated through under-sampling of the drive signal, is at the same frequency and phase as the oscillation generated by NCO1.

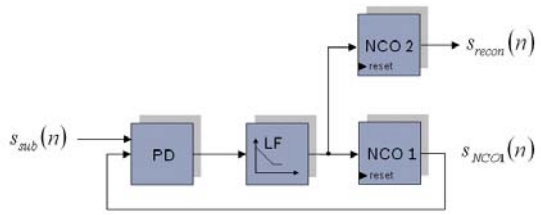

Fig. 7. Under-sampling filter with the two NCOs for signal reconstruction

As pointed out in Fig. 5 and equation (6), the two center frequencies of the NCOs are coupled. The frequency of each NCO is dependent on the given phase increment PI, the cycle time of the NCO T_{NCO}, and the accumulator word length N_{akku}. To regulate small changes in frequency, the phase increments of NCO1 and NCO2 are chosen in such a way that they follow an inversely proportional relationship shown in Fig. 8. ω_{NCO1} and ω_{NCO2} denote the angular frequency of the respective numerical oscillator. ω_{M1} and ω_{M2} denote their center frequencies.

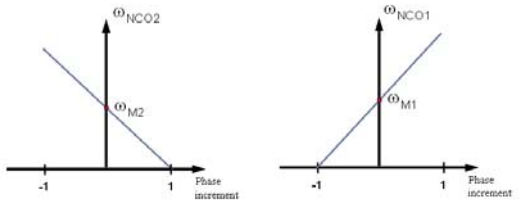

Fig. 8. Anti-proportional coupling of the two numerical oscillators

That means that a frequency change of the under-sampled drive signal $s_{sub}(n)$ compared to the center frequency of NCO1 has the same frequency shift as the center frequency of NCO2 compared to the output frequency of NCO2. As shown in Fig. 7, the NCO2 is used to reconstruct the original drive signal. If the two center frequencies are chosen in accordance to the above mentioned conditions, every frequency change of the NCOs, indicated through a change of the original drive signal $s_{drive}(t)$, has a symmetrical consequence and provides a reconstructed signal $s_{recon}(n)$ with a frequency shift of the same absolute value.

IV. Measurements

Fig. 9 shows the measurement results of the under-sampling filter approach. For the measurements presented in this section the drive path was measured with open loop. That means that the output of the AGC was not fed back to excite the sensor element. The purpose of these measurements were to proof the functionality of the developed system realization presented in this paper.

The under-sampled and filtered input signal $s_{sub}(n)$ is shown in Fig. 9. The PLL is synchronized and therefore the signal $s_{NCO1}(n)$ is at the same phase and frequency like the under-sampled input signal $s_{sub}(n)$. Because of the coupling

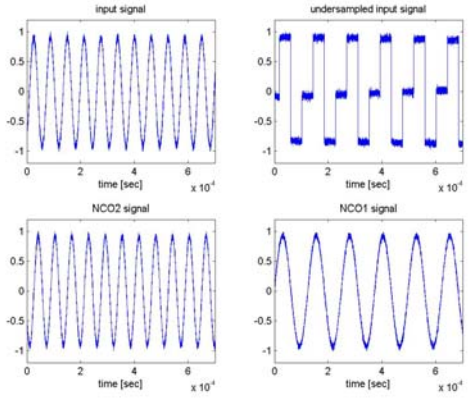

Fig. 9. Measurement results of the system realization with the parameters: $f_{drive} = 16.0kHz$, $f_A = 24.0kHz$

of NCO1 with NCO2 the output of NCO2 reconstructs the given input signal shown in Fig. 9. The signal $s_{recon}(n)$ is at the same frequency as the given input signal $s_{drive}(n)$. However, as pointed out in Fig. 9, there is still a phase inaccuracy between both signals. At this it is assumed that a closed loop configuration will operate more stable. This has to be examined in future work.

V. Conclusion

A system realization to reconstruct the sinusoidal signal of the drive frame excitation of a micromachined yaw rate sensor is presented. The presented system works with an under-sampling approach. It is shown that it is possible to sample and reconstruct the drive signal of the micromechanical sensor with sample frequencies below the Nyquist limit. With the use of this system, it is possible to operate the analog part of the sensor element in a power saving mode. The system approach was realized on a FPGA and proper operation could be demonstrated. For future refinement and improvement some problems arising from phase inaccuracy will have to be solved and the noise behavior has to be analyzed.

References

[1] A. Lawrence, *Modern Inertial Technology*, Navigation Guidance and Control, Springer-Verlag New York, 2002
[2] W.M. Macek and D.T.M. Davis, *Rotation rate sensing with traveling wave ring lasers*, Appl. Phys. Lett. 2, Springer-Verlag New York, 1. Feb. 1963, pp67-68
[3] J. Bernstein, et al., *A micromachined comb-drive tuning fork gyroscope*, IEEE Micro Electro Mechanical Systems, IEEE Catalog No. 93CH3265-6, Feb. 1993, pp143-148
[4] M. Palaniapan, R.T. Howe, J. Yasaitis, *Integrated surface-micromachined z-axis frame microgyroscope*, Electron Devices Meeting, 2002. IEDM '02. Digest. International, Dec. 2002, pp203-206
[5] K. Funk, H. Emmerich, A. Schilp, M. Offenberg, R. Neul, F. Lärmer, *A surface micromachined silicon gyroscope using a thick polysilicon layer.*, Proc., Twelfth IEEE Int. Conf. on Micro Electro Mechanical Systems (MEMS '99), Jan. 17–21, Orlando, Fla., pp57–60
[6] R. Neul, U. Gómez, K. Kehr, W. Bauer, J. Classen, C. Döring, E. Esch, S. Götz, J. Hauer, B. Kuhlmann, C. Lang, M. Veith and R. Willig, *Micromachined Gyros for automotive applications*, Sensors 2005 IEEE, Oct. 2005, pp527-530
[7] R. E. Best, *Theorie und Anwendung des Phase-locked Loops*, 5rd ed. AT-Verlag Aarau, 1992
[8] U. Kiencke and H. Jäckel, *Signale und Systeme*, 2rd ed. Oldenburg Verlag München, Sep.2002